Aluminum nitride integrated photonics for far-UVC second harmonic generation: recent advances and future outlook

Brent Fisher[a ✝], John Carlson[a], Wei Jiang[a], Konrad Ziegler[a], Perry Wang[a], Jacob Davis[a], Jim Carter[a], Tinh Tran[a], Scott Burroughs[a]

(a) Uviquity Inc, 1017 Main Campus Drive, Suite 2300, Raleigh, NC, 27606, United States

(✝) corresponding author: brent.fisher@uviquity.com

ABSTRACT

Infectious disease is a massive health and economic burden on society, necessitating new approaches for mitigation. Disinfection using Far-UVC light (λ<230nm) offers a solution that is both effective against pathogens and safe for human exposure, but no low-cost solid-state sources of far-UVC light are commercially available. This paper reports on the development of efficient, low-cost, fully solid-state far-UVC light engines based on Aluminum Nitride (AlN) waveguides. We use nonlinear frequency conversion, specifically Second Harmonic Generation (SHG), to convert pump light from mature blue laser diodes into far-UVC light. We describe the design and fabrication of the AlN photonics platform, utilizing MOCVD epitaxial growth and lithography to achieve high-quality waveguides. We demonstrate broadband frequency conversion across the UVC spectrum, achieving coverage between 214 nm and 232 nm. Furthermore, we present the first integration of a commercial diode laser with an AlN SHG converter in a hybrid optical package. Experimental results show exponential improvements in signal generation through process optimization, our first steps toward scaling this platform for widespread disinfection applications.

Keywords: Far-UVC, Aluminum Nitride, Second Harmonic Generation, Integrated Photonics, Waveguides, MOCVD, Disinfection, Nonlinear Optics

---

1. INTRODUCTION

Infectious diseases remain a persistent threat to global health. While traditional antibiotics and vaccines are vital, increasing resistance and the emergence of new viral strains highlight the need for alternative mitigation strategies [1]. Ultraviolet (UV) light is a well-established disinfectant. However, conventional germicidal UV (λ>240nm) is hazardous to human skin and eyes. Recent research has shown that a specific portion of the spectrum, far-UVC light (λ<230nm), is safe for human exposure while retaining high efficacy against pathogens[1,2]. The safety mechanism is based on length scales: biological materials, including skin, possess high optical absorption at these wavelengths. Consequently, the stratum corneum (outer layer of human skin consisting of dead skin cells) absorbs the far-UVC light before it reaches living cells [1,2]. In contrast, pathogens do not have protective cells and are thus inactivated by the same light.

Current technologies for generating far-UVC are limited. Lamps based on gas-phase atomic transitions (e.g., KrCl excimer) are the only practical commercialized option, but these are expensive, are limited to large form factors, require high voltages and they operate with less than 1% wall plug efficiency. Direct emission from solid-state materials, such as LEDs, faces significant materials science challenges, emit undesirably broad spectral emission,

and have thus far, demonstrated very low efficiency at wavelengths below 250 nm[3].

A third approach, based upon nonlinear frequency conversion, is the focus of this work. Leveraging mature, mass-produced blue laser diodes, we can generate far-UVC light through Second Harmonic Generation (SHG) in a solid-state platform. This approach offers a scalable, compact, and robust solution for producing far-UVC light.

2. METHODOLOGY AND MATERIAL SELECTION

2.1 Modal Phase Matching for Second Harmonic Generation

Second Harmonic Generation relies on the nonlinear response of a material to combine the energy of two pump photons at frequency ω into a single photon at frequency 2ω. An expression for the second harmonic (SH) converted power at a single wavelength ($\omega \rightarrow 2\omega$) in the presence of optical loss in a waveguide is:

$$P_{SH} = \frac{\left(\xi^2/A_{WG}\right)\left(2d_{xx}^2\,\omega_{SH}^2\right)}{\left(\varepsilon_0 n_1^2 n_{SH} c^3\right)} \; \frac{P_0^2 L^2 e^{-\alpha_{SH}L}\left(\left(e^{\Delta\alpha L}-1\right)^2+4e^{\Delta\alpha L}sin^2(\Delta kL/2)\right)}{\left((\Delta\alpha L)^2+(\Delta kL)^2\right)}$$

where

- P_0 is the pump power,
- d_{xx} is the nonlinear response of the material at the appropriate polarization,
- ξ^2 is the square of the spatial overlap between waves at ω and 2ω,
- L is the length of the nonlinear interaction (overlap of the two waves)
- A_{wg} is the cross sectional area of the waveguide,
- α_{SH} is the optical loss at the second harmonic wavelength
- $\Delta\alpha = \alpha_{SH}/2 - \alpha_0$ represents the difference between loss at SH (α_{SH}) and the pump (α_0), and,
- $\Delta k = k_{SH} - 2k_0$ represents the phase mismatch between waves at ω and 2ω.

In the absence of phase matching $\Delta k = 0$, the second-harmonic photons dephase, preventing signal accumulation[4]. This behavior is captured by the $sin^2(\Delta kL/2)/(\Delta kL/2)$ factor on the right hand side of the equation above. While techniques such as birefringence phase matching and quasi-phase matching (QPM) are common in free-space optics, the use of waveguides by integrated photonics allows for modal phase matching. In a waveguide, the effective refractive index of a guided mode is determined by the geometric dimensions (width and height). Therefore, by careful design of the geometry, we can match the effective index of a fundamental mode (at ω) to that of a higher-order mode (at 2ω), to achieve phase matching and enable efficient power transfer. Our design leverages modal phase matching between the TM_{00} mode for the pump and either the TM_{40} or the TM_{04} at the second harmonic frequency.

2.2 Aluminum Nitride (AlN) Material System

Numerous studies have been reported over the past decade attesting to the beneficial properties of AlN integrated photonics [5-11]. Aluminum Nitride (AlN) was selected as the nonlinear material for this platform because of several advantageous properties: **(1) Transparency:** A wide bandgap (6.2 eV) ensures transparency down to near 200 nm, spanning the far-UVC window. **(2) Refractive Index:** A high index ($n \sim 2.2$) allows for tight mode confinement and high optical intensity. (3) **Nonlinearity:** The second-order nonlinear coefficient ($d_{33} \sim 4.3$pm/V) is relatively strong, second only to BBO among transparent crystals in this range. Furthermore, doping with Sc can increase this coefficient by more than an order of magnitude[12]. **(4) Scalability:** Unlike more familiar nonlinear crystals like BBO, KDP, LBO, etc, AlN is compatible with standard III-N semiconductor fabrication infrastructure. This means

not only is it possible to fabricate waveguides, but the resulting process can be done at wafer scale and easily ported to existing large scale foundries, leading to rapidly scalable high volume manufacturing at low cost.

3. FABRICATION

We utilize Metal-Organic Chemical Vapor Deposition (MOCVD) to grow high-quality, single-crystal AlN thin films on sapphire substrates. Compared to sputtered films, which are often polycrystalline and lossy, MOCVD provides a single crystal such that the crystalline orientation is constant throughout the waveguide, making the nonlinear interaction more efficient. We found the intrinsic loss of our AlN films to be approximately 2.7 dB/cm at 447 nm based on the Metricon prism coupling method. This loss is driven in part by surface roughness which we measured by Atomic Force Microscopy (AFM) to be approximately ~ 0.5nm RMS.

Fabrication of AlN on sapphire waveguides proceeds by the following steps, as depicted in figure 1:

1. Deposition of an oxide hard mask.
2. E-beam lithography to define the waveguide patterns.
3. Transfer of the pattern to the hard mask via etching.
4. Dry etching of the AlN film to define the waveguides.
5. Removal of the hard mask and deposition of an SiO_2 cladding.

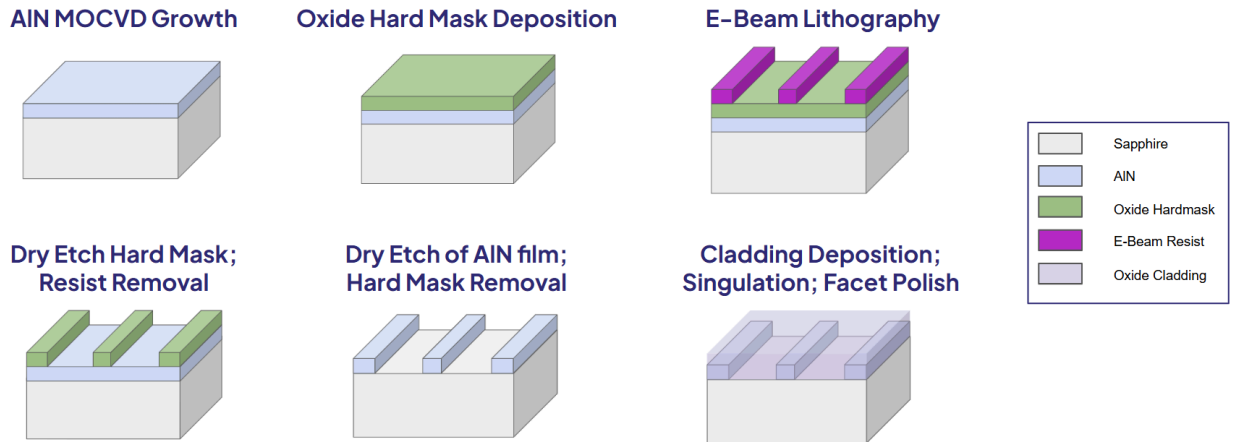

Figure 1 – Process flow for fabrication of AlN on Sapphire waveguides

4. RESULTS

4.1 Broadband Far-UVC Generation

We have successfully demonstrated SHG in AlN waveguides across a range of blue pump wavelengths using Ti:Sapphire, distributed feedback (DFB), and Fabry-Perot diode laser sources. By varying the waveguide dimensions to satisfy phase-matching conditions, we generated far-UVC light spanning 214 nm to 233 nm. These results, shown in figure 2, represent the shortest reported wavelengths generated by SHG in AlN waveguides.

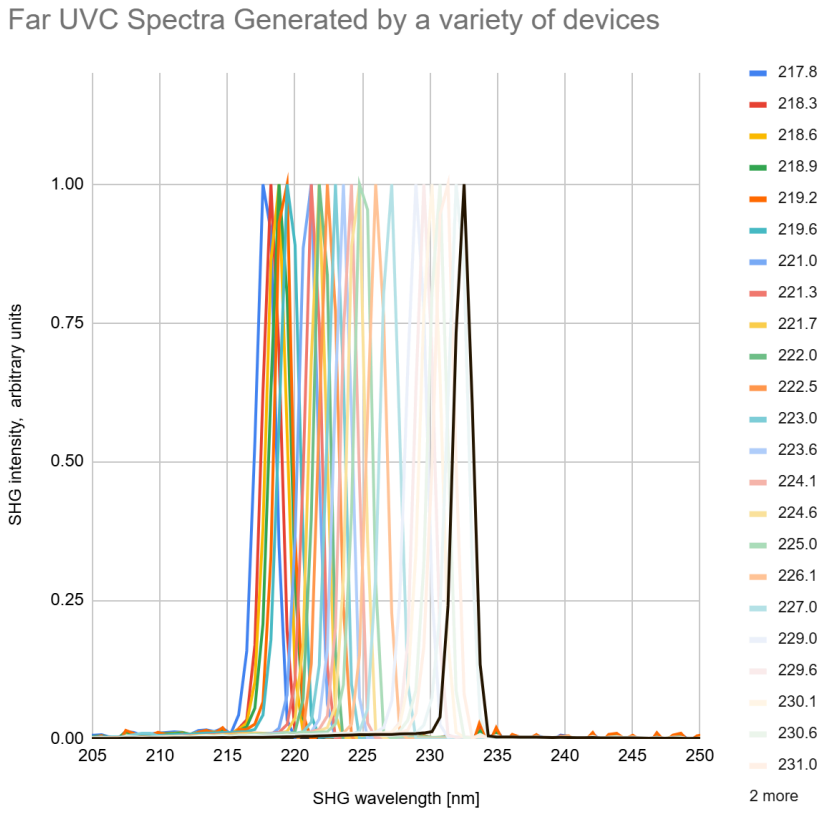

Figure 2 – Far-UVC emission spectra for waveguides designed for a range of wavelengths from 217nm to 232nm (black curve).

4.2 Mode Identification

The waveguide geometries that we targeted for initial SHG at far-UVC (width and thickness between 300 and 400nm), support two distinct modes that are candidates to provide phase matching at far-UVC: TM_{04} and TM_{40}. Between these two alternatives, TM_{04} mode is preferred because we expect it to exhibit less interaction with sidewall roughness and also to accommodate phase matching at wider geometries where pump loss may be lower. Additionally, TM_{04} is better suited to efficiency enhancements like polarity inversion as described by Honda et al.[13]

In order to verify the active mode, we analyzed the dependence of the optimal SHG wavelength design on waveguide geometry. The TM_{04} mode is highly sensitive to waveguide thickness but insensitive to waveguide width, In contrast, the phase matching wavelength of the TM_{40} mode is highly sensitive to width. The difference in these width dependencies provided the basis for us to verify that our waveguides in fact leverage the TM_{40} mode. This is illustrated by figure 3 where experimental data from more than fifty waveguides whose widths varied from 280nm to 480nm exhibit practically no variation of optimal SHG wavelength across the full range of widths. This behavior is consistent with the TM_{04} mode as indicated by the red line.

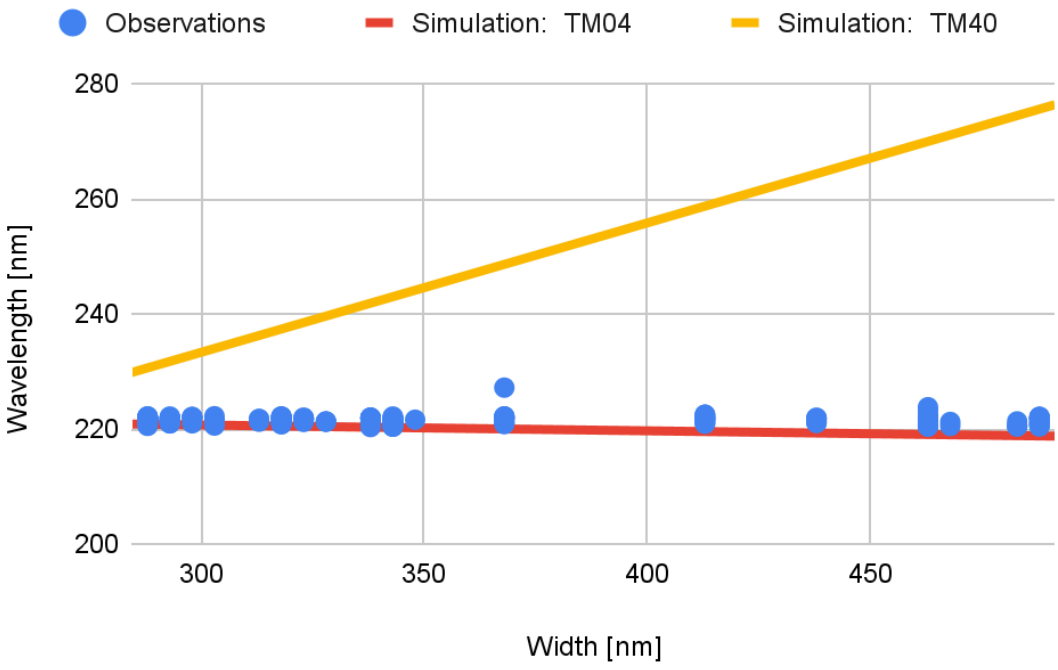

Figure 3 – Simulated (red, yellow) and measured (blue) dependence of optimal SHG wavelength on waveguide width

4.3 Performance Improvements and Prototyping

Over four generations of device fabrication completed in the past half year, we have observed exponential improvements in SHG signal intensity, which is depicted in figure 4. We attribute these gains to (1) optimized waveguide geometry, (2) improved facet quality for better input coupling, and (3) reduced propagation loss obtained by process refinement. The SEM micrographs in Figure 5 provide an indication of the improvement of the waveguides. The first image comes from a sample from Run 2 while the second SEM image comes from samples produced by our most recent processing runs.

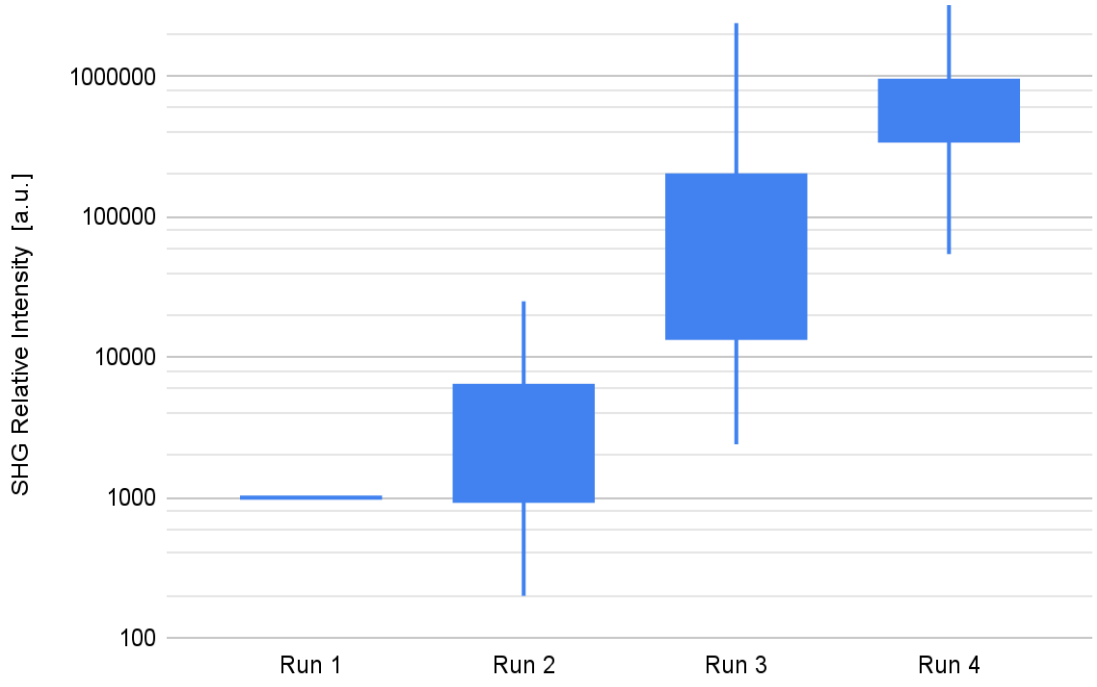

Figure 4 – Relative increase of SHG efficiency and power output access four generations of fabrication

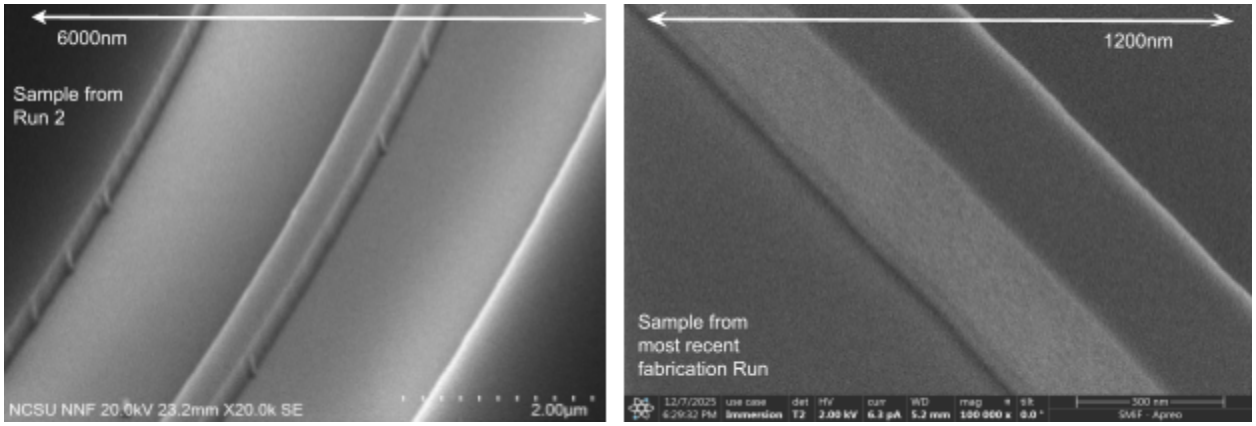

Figure 5 – SEM images of waveguides produced from two separate processing runs. Note the 5x greater scale on the right.

Building upon our device level improvements, we have integrated AlN waveguides into a single package as shown in figure 6. This small prototype (2 x 5 x 7 cm) uses micro-optics to efficiently couple light from a commercial diode laser into the AlN waveguide chip for SHG conversion. The far-UVC light that is generated exits the AlN chip and is collected by a high NA lens. A diffraction grating is used to separate the emitted far-UVC light from the residual blue pump light, achieving SHG levels exceeding levels observed in our benchtop experiments.

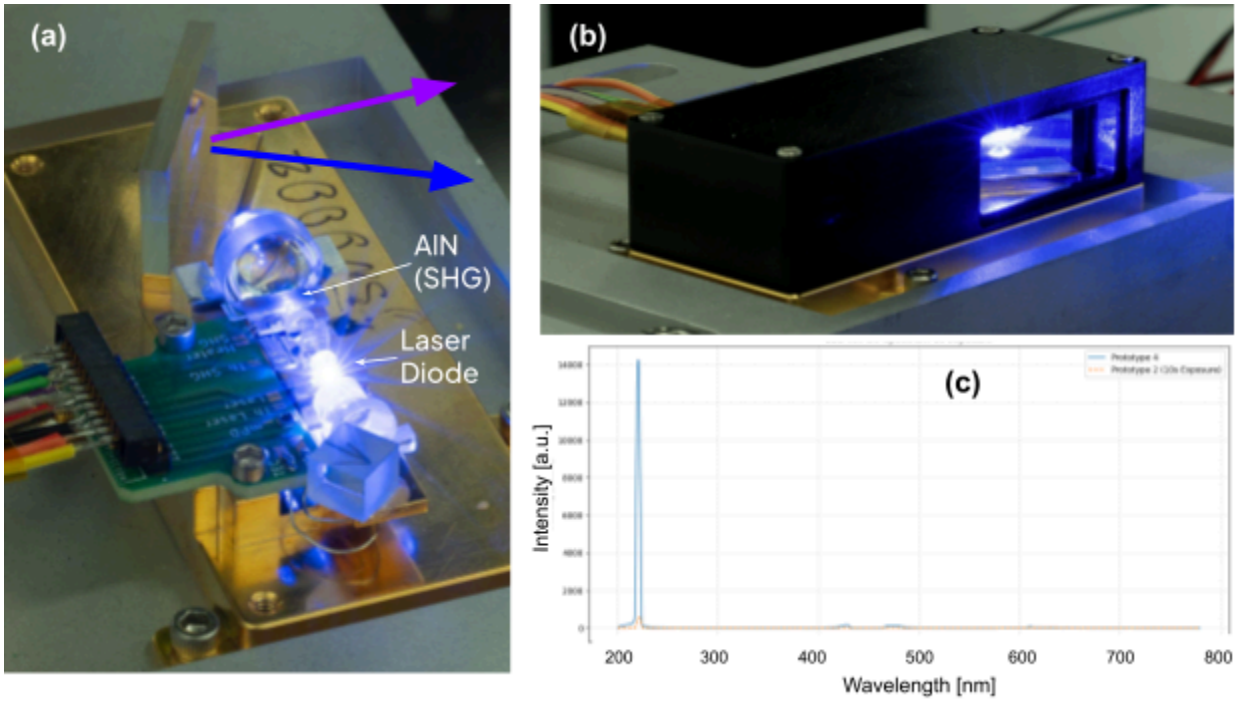

Figure 6 – Photographs of prototype SHG generation package with far-UVC emission: (a) shows the interior micro-optics in operation with the blue laser diode coupled to the AlN chip for SHG; (b) shows the package with the cover in place. (c) The (filtered) emission spectrum is shown in the lower right.

5. FUTURE OPPORTUNITIES

Significant potential remains for increasing the SHG conversion efficiency of our AlN platform in the near term, including:

- **Waveguide Loss Reduction:** Near term opportunity to reduce blue light propagation loss of our waveguides (inclusive of intrinsic and scattering) to <4 dB/cm, in line with best-in-class results[7-11].
- **Inverted Polarity:** Polarity inversion of the AlN can substantially increase the overlap integral between the pump and second-harmonic modes[13] thereby enabling significantly increased SHG conversion efficiency.
- **Material Enhancement:** Scandium (Sc) doping of AlN can increase the piezoelectric and nonlinear coefficients by up to 12x which can unlock further increases in efficiency[12].
- **Heterogeneous Integration:** Uviquity's medium term roadmap seeks to integrate GaN lasers directly onto the AlN platform in a single chip. Not only will this reduce coupling losses for a single pass SHG design, but it opens up the possibility of intracavity designs where much higher pump intensities may be realized.

6. CONCLUSION

We have developed a low-loss, integrated AlN-on-sapphire photonics platform capable of generating human-safe far-UVC light. We demonstrated frequency conversion spanning the far-UVC spectrum with results ranging from 214 nm to 232 nm. Through iterative process improvements, we achieved orders-of-magnitude performance gains and successfully integrated the technology into a compact hybrid package. These results validate the viability of nonlinear AlN waveguides as a scalable solution for next-generation disinfection technology.

7. REFERENCES

1. Buonanno, M. et al., "207-nm UV light - a promising tool for safe low-cost reduction of surgical site infections. I: in vitro studies," PLoS One 8, e76968 (2013).
2. Eadie, E. et al., "Far-UVC (222 nm) efficiently inactivates an airborne pathogen in a room-sized chamber," Sci. Rep. 12, 4373 (2022).
3. Amano H., et al., "The 2020 UV emitter roadmap", J. Phys. D: Appl. Phys. 53 (2020) 503001 (57pp)
4. Boyd, R., [Nonlinear Optics], 3rd ed., Academic Press (2008).
5. He, J. et al., "Nonlinear nanophotonic devices in the ultraviolet to visible wavelength range," Nanophotonics 9, 3781 (2020).
6. Li, N. et al., "Aluminium nitride integrated photonics: a review," Nanophotonics 10, 2347 (2021).
7. Liu, X. et al., "Aluminum nitride photonic integrated circuits: from piezo-optomechanics to nonlinear optics" Adv. Opt. Photonics 15, 236 (2023).
8. Stegmaier, M. et al., "Aluminum nitride nanophotonic circuits operating at ultraviolet wavelengths," Appl. Phys. Lett. 104, 091108 (2014).
9. Lu, T-J. et al., "Aluminum nitride integrated photonics platform for the ultraviolet to visible spectrum," Opt. Exp. 26, 11147 (2018).
10. Liu, X. et al., "Ultra-high-Q UV microring resonators based on a single-crystalline AlN platform," Optica 5, 1279 (2018).
11. Shin, W. et al., "Demonstration of green and UV wavelength high Q aluminum nitride on sapphire microring resonators integrated with microheaters," Appl. Phys. Lett. 118, 211103 (2021).
12. Yoshioka, V., et al., "Strongly enhanced second-order optical nonlinearity in CMOS-compatible $Al_{1-x}Sc_xN$ thin films" APL Mater. 9, 101104 (2021).
13. Honda H., et al., "229 nm far-ultraviolet second harmonic generation in a vertical polarity inverted AlN bilayer channel waveguide," Appl. Phys. Express 16 062006, (2023).

Brent Fisher, John Carlson, Wei Jiang, Konrad Ziegler, Perry Wang, Jacob Davis, Jim Carter, Tinh Tran, Scott Burroughs, "Aluminum nitride integrated photonics for far-UVC second harmonic generation: recent advances and future outlook," Proc. SPIE 13890, Physics and Simulation of Optoelectronic Devices XXXIV, 1389009 (2026) https://doi.org/10.1117/12.3080065